THE ASTROPHYSICAL JOURNAL, 511:436–450, 1999 January 20

TEMPORAL EVOLUTION OF FINE STRUCTURES IN AND AROUND SOLAR PORES

MICHAL SOBOTKA,[1] MANUEL VÁZQUEZ,[2] JOSÉ ANTONIO BONET,[2] ARNOLD HANSLMEIER,[3] AND JOHANN HIRZBERGER[3]

Received 1998 June 1; accepted 1998 August 26

ABSTRACT

Time series of high-resolution white-light images of six solar pores, observed in 1993 and 1995 at the Swedish Vacuum Solar Telescope (La Palma), are analyzed. The pores constitute an almost ideal laboratory in which to study the interaction of a vertical magnetic field with surrounding convective motions, without the perturbation of the inclined magnetic field in the penumbra. Umbral dots observed in a large ($D = 8''.9$) pore are similar to those in mature umbrae, but they live longer, are brighter, and have a higher filling factor. Granular motions in the vicinity of pores are driven by mesogranular flows. Motions toward the pore dominate in the 2″ zone around the pore boundary, while at larger distances the granules move away from the pore. Pushed by these motions, small granules and granular fragments located close to the pore border sometimes penetrate into the pore, where they move inward as bright short-lived features very similar to umbral dots. The capture of bright features by the pore is probably a microscale manifestation of the "turbulent erosion," which results in the decay of the pore. Formation of a transitory penumbra-like structure at the border of the large pore was observed simultaneously with the appearance of expanding elongated granules, separated by dark filaments, in an adjacent granular field. These effects can be interpreted as a consequence of emerging bipolar magnetic "loops" caused by a temporary protrusion of opposite magnetic polarity.

Subject headings: Sun: activity — Sun: granulation — Sun: magnetic fields — sunspots

1. INTRODUCTION

Solar pores are sunspots lacking penumbrae and constitute the first stage of sunspot evolution. They provide, therefore, an essential key to understanding the mechanism driving the emergence of magnetic flux at small spatial scales and provide information on how this process affects the superficial convective structures. Because of the absence of the perturbing penumbra, pores constitute a virtually ideal laboratory in which to study the interaction between the vertical magnetic field, forming the umbra, and the surrounding convective motions. Muller (1992), Soltau (1994), and Sobotka (1997) have reviewed the results of sunspot observations with high spatial resolution. In this paper we follow the nomenclature of fine structures proposed by Sobotka, Bonet, & Vázquez (1993).

Differences in average thermal properties have been found between small and large sunspots (e.g., Sobotka 1985; Collados et al. 1994). Similar differences and analogies can be found between pores and sunspots. Muglach, Solanki, & Livingston (1994), observing solar pores in the infrared, determined that the intensity–to–magnetic field relation was similar to that measured by Kopp & Rabin (1992) for evolved sunspots: Regions with higher magnetic field strength were darker and cooler than those with lower field strength. Although the pores have mainly vertical magnetic lines, canopies have been observed above them (Keppens & Martínez Pillet 1996; Sütterlin, Schröter, & Muglach 1996; Martínez Pillet 1997; Sütterlin 1998).

Bonet, Sobotka, & Vázquez (1995) made a detailed photometric study of fine structures inside pores using eclipse observations. Umbral dots (hereafter UDs) in a pore were similar to those in evolved spots, but their sizes seemed to be larger. As far as we know, no measurements exist for the lifetimes of UDs in pores. For evolved sunspots, the first estimates of lifetimes led to about 25 minutes (Beckers & Schröter 1968; Adjabshirzadeh & Koutchmy 1980). Later Kitai (1986) and Kusoffsky & Lundstedt (1986) indicated that the typical lifetime could be longer: 40 and 60 minutes, respectively. Ewell (1992) reported a mean lifetime of only 15 minutes. Several UDs were observed to exist for more than 2 hours (Kusoffsky & Lundstedt 1986; Ewell 1992). However, recently Sobotka, Brandt, & Simon (1997a, 1997b) showed that there are no privileged sizes and lifetimes for UDs—the number of UDs increased with decreasing size and lifetime. Moreover, they did not find any clear difference in proper motions of central and peripheral UDs, which has been reported previously by Ewell (1992).

Penumbral grains have been observed to move toward the umbra with an average speed of 0.3–0.5 km s^{-1} (Muller 1973, 1976; Tönjes & Wöhl 1982; Wang & Zirin 1992; Molowny-Horas 1994). Jahn (1997) and Schlichenmaier, Jahn, & Schmidt (1998) suggested a model of a thin magnetic flux tube in the penumbra, which attempts to explain this motion. Some penumbral grains cross the umbral border and continue to move as UDs (Sobotka et al. 1995a). There is an interesting question as to whether an analogous process, taking place at the pore boundary, may relate UDs inside the pore with photospheric granules.

Another question concerns the motions of granules in the vicinity of pores. Muller & Mena (1987) found that facular points and granules move away from a decaying sunspot. This effect was observed also in stable spots (Shine et al. 1987). In contrast to the sunspot observations, Wang & Zirin (1992) reported converging flows around pores with speeds of 0.5 km s^{-1} and coherence scales of 2000–3000 km. However, Denker (1998) did not find this type of motion in a series of speckle-reconstructed images.

A related problem is how the granulation is affected by the emergence of new magnetic flux or by the formation of a horizontal magnetic field inside the active region. Miller

[1] Astronomical Institute, Academy of Sciences of the Czech Republic, 25165 Ondřejov, The Czech Republic.
[2] Instituto de Astrofísica de Canarias, 38200 La Laguna, Spain.
[3] Institut für Astronomie, Universitätsplatz 5, 8010 Graz, Austria.

(1960) first detected an alignment of granules. The longest alignment of intergranular lanes that Brants & Steenbeek (1985) found spanned 7200 km and lasted 10 minutes. Tarbell et al. (1990) observed dark alignments with typical lengths of 1500–4000 km. According to Wang & Zirin (1992), dark alignments either connect magnetic elements of opposite polarity or correspond to unipolar fields. It is also well known that the properties of the granulation are affected by the magnetic field in plage regions, giving rise to abnormal granulation (cf. Sobotka, Bonet, & Vázquez 1994).

An important step in the evolution of sunspots is the penumbra formation. This process has scarcely been studied in the past because of the inherent difficulties of observation. Bray & Loughhead (1964) described the formation of a transitory penumbra living less than 3 hours, produced by the darkening of intergranular patches. Bumba & Suda (1984) pointed out that the process of penumbra formation is a continuous reorganization of granular areas and commented that the penumbra does not develop in such areas of the spot, where the lines of force cannot connect fields of opposite polarity. Penumbral fibrils develop from the normal granulation, and they may be transformed back to it.

From the theoretical point of view, it is critical to know under which conditions the field lines become more horizontal, transforming the pore to a sunspot. Simon & Weiss (1970) established the distinction between pores and sunspots for a critical flux of 10^{20} Mx, corresponding to a radius of $\simeq 1500$ km. Mullan (1983) noted the importance of a critical fanning out of the penumbral lines of force to get stability and proposed that the spot radius, R, should be larger than the pressure scale height, H_p, which is 230 km for the penumbra (Collados, del Toro Iniesta, & Vázquez 1987). Zwaan & Cram (1989) claimed that the ratio R/H_p is a function of the magnetic flux and that the division between pores and sunspots appears for a value of about 13. Rucklidge, Schmidt, & Weiss (1995) developed a model of the transition between pores and sunspots, showing that the penumbral mode of convection sets in abruptly and rapidly. Leka & Skumanich (1998) analyzed the vector magnetic field of a rudimentary penumbra obtained with the Advanced Stokes Polarimeter. They determined the critical flux of (1–1.5) $\times$ 10^{20} Mx above which a partial penumbra may develop. The appearance of the penumbra was preceded by an increase of magnetic field strength and filling factor and by a decrease of continuum intensity in the pore.

In this paper we use two time series of images, obtained in very good seeing conditions at the Swedish Vacuum Solar Telescope at the Roque de los Muchachos Observatory (La Palma), to study the photometric properties of fine structures in and around solar pores, their temporal evolution, and the fields of proper motions. We were fortunate to observe the evolution of a large pore with a lot of bright features inside, to track in detail horizontal motions of granules and their fragments around the pores, and to detect temporary reconfigurations of intensity patterns at the border of the large pore and in the surrounding granular field.

2. OBSERVATIONS

Time series of white-light images of the active regions presented in Table 1 were obtained in the years 1993 and 1995 at the Swedish Vacuum Solar Telescope (Roque de los Muchachos Observatory, La Palma; see Scharmer et al. 1985). This 50 cm aperture telescope gives a scale of 9.″22 mm^{-1} at the primary focus, where an 8 bit Kodak Megaplus Model 1.4 CCD camera of 1360 $\times$ 1036 pixels (image scale of 0.″062 $pixel^{-1}$) was used with a typical exposure time of 11 ms. The system was configured to work as a real time frame-selection device with selection intervals of 15 s. Storing the data on the disk took 4–5 s, so that the average intervals between the frames were 19–20 s.

For the observing run in 1995 a second Megaplus 1.4 CCD camera was installed to take frames in the G band using a filter centered at $\lambda = 430.8$ nm with an FWHM of 1.1 nm. The exposures were synchronized with the white-light camera, and the frame selection system used the white-light images. Because of the narrow bandpass and low spectral sensitivity of the CCD detector in the G band, it was necessary to set the gain of the G-band camera 12 dB higher than that of the white-light one to keep the exposure times of both cameras approximately equal. The consequence was stronger electronic noise in the G-band camera (rms value ± 3 count, that is, $\pm 1.5\%$ of the mean photospheric intensity) compared with that of the white-light (± 0.6 counts, ± 0.3 %).

The typical value of the granulation contrast, determined from white-light images in a field far away from any activity, was 7.6% without any corrections applied. Many images show details of granular structure near the diffraction limit of the telescope (0.″27). The level of scattered light was estimated to be less than 1% of the mean photospheric intensity (cf. Sobotka et al. 1993; Bonet et al. 1995). In the 1995 series, the telescope drifts and low-frequency components of image motion due to seeing were minimized using a quad-cell sunspot tracker.

Time series of two young active regions were used for this study. In 1993, a very small region, Ramy 174 (Solar Geophysical Data No. 588), consisting of two small pores (P1, P2), appeared only on the day of observation (June 18). It was located close to the disk center at the heliocentric position $\mu = 0.97$.

The second active region, NOAA 7886, was born on 1995 June 29 (Solar Geophysical Data No. 612) and observed as a group of rapidly developing pores on the next day. It disappeared on July 1. On June 30 it was located in the central zone of the disk at the heliocentric position $\mu = 0.92$.

TABLE 1

GENERAL CHARACTERISTICS OF TIME SERIES

Date	Region	Pores	λ (FWHM) (nm)	Mean Time Spacing (s)	Duration (minutes)	G-band?
1993 Jun 18.....	Ramy 174	P1, P2	525.7 (5.8)	19	85	No
1995 Jun 30.....	NOAA 7886	P3, P4 P5, P6	542.5 (10)	20	67	Yes

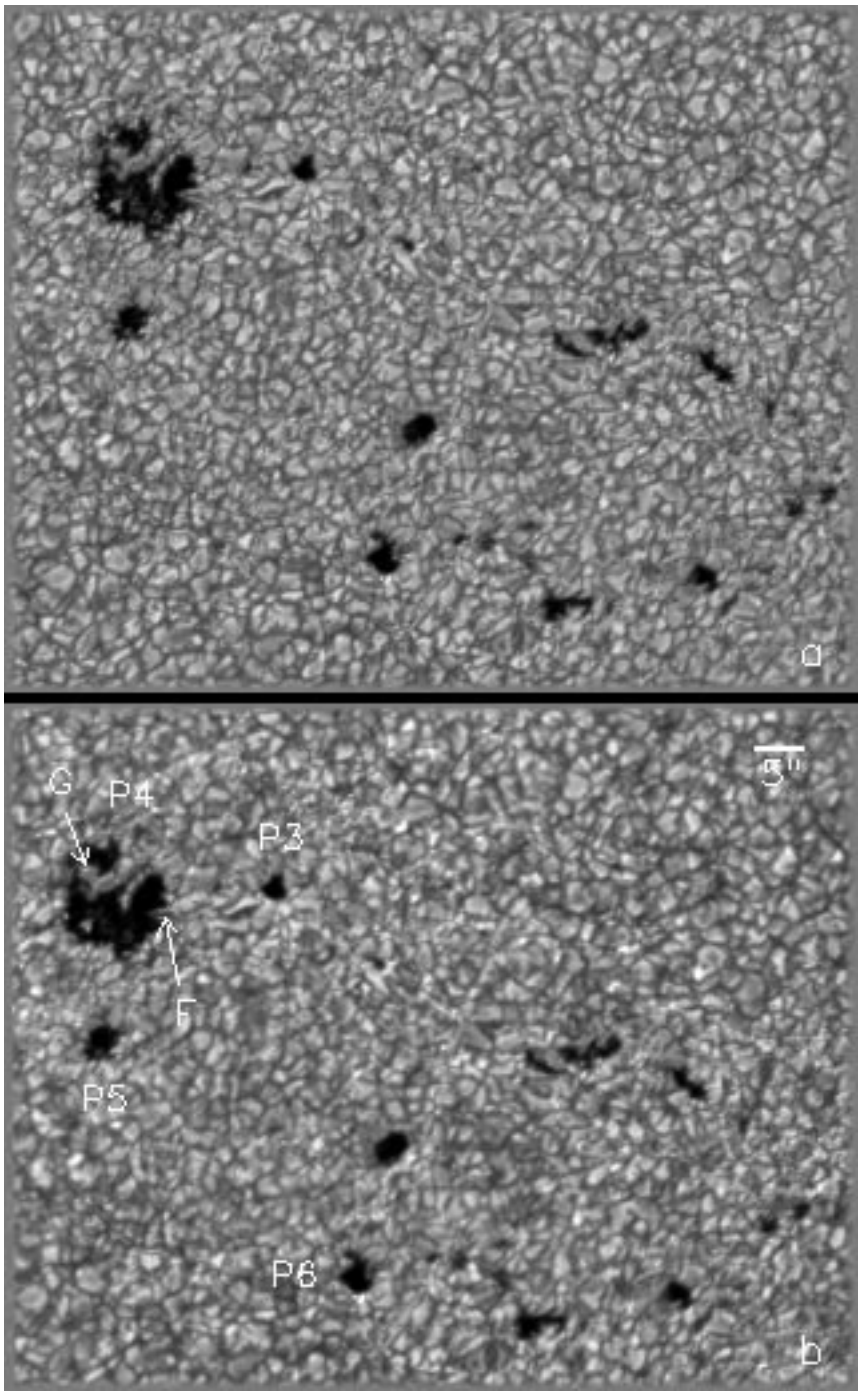

FIG. 1.—Pictures showing the observed region NOAA 7886 on 1995 June 30 (*a*) in white light (542.5 nm) and (*b*) in the *G* band (430.8 nm). The pores under study are indicated as P3–P6. The arrows show the growing "granule" (G) and the location of the penumbra-like filamentary structure (F) in P4.

Figure 1 shows a representative view of the whole region, where the pores under investigation are indicated as P3–P6. Two different systems with *opposite* magnetic polarity were observed:

1. Seven to eight pores (including P6) assembled in a roundish structure typical for emerging regions.

2. Three isolated pores P3–P5 including a very large one (P4), with a diameter of 8".9, showing a large variety of fine bright structures (UDs and two light bridges). The pore P4 can be considered an extraordinary object, because of both the size (close to the maximum observed sizes for pores) and the richness of its internal structure. Probably, because of the latter, the pore lived only 3 days.

Magnetic maps of the active region NOAA 7886 were obtained on June 30 at the photoelectric scanning magnetograph of the Ondřejov Observatory (Klvaňa & Bumba 1994). The maximum field strength in P4 was approximately 1000 G (V. Bumba & M. Klvaňa 1998, private communication). Complementary data were also taken from the NSO/Kitt Peak magnetograms.

3. DATA ANALYSIS

3.1. *Image Processing*

After dark-current and flat-field corrections, we derotated the frames to compensate for the rotation of the field of view introduced by the optical system of the telescope. The average photospheric intensity $I_{\rm phot}$ in all frames was normalized to unity to compensate for changes of transparency and/or exposure time. The frames were then registered to remove large-scale image motions (rigid alignment).

The correction for the theoretical instrumental profile of the telescope and the noise filtering were carried out simultaneously in the central area of 1280 × 1032 pixels applying the Wiener filter

$$F(\nu) = \frac{M(\nu)}{M^2(\nu) + [P_S(\nu)/P_N(\nu)]^{-1}}\,, \tag{1}$$

where $M(\nu)$ is the modulation transfer function (MTF) of the diffraction-limited 50 cm objective, ν the spatial frequency in the Fourier domain, and $P_S(\nu)/P_N(\nu)$ is the signal-to-noise power ratio. Since the signal-to-noise ratio of the *G*-band camera decreased with ν because of enhanced electronic noise at the highest frequencies, we were forced to model the frequency variation of $P_S(\nu)/P_N(\nu)$ using an approximation suggested by Collados & Vázquez (1987) and obtained the Wiener filter in the form

$$F(\nu) = 1/M(\nu) \quad \text{for } \nu \le \nu_0\,, \tag{2}$$

$$F(\nu) = \frac{M(\nu)}{M^2(\nu) + K(\nu - \nu_0)} \quad \text{for } \nu > \nu_0\,. \tag{3}$$

The parameters ν_0 and K were determined by trial and error to achieve a maximum restoration together with the minimization of noise in the *G*-band frames. The values $\nu_0 = 2.1$ arcsec^{-1} and $K = 0.01$ were the best in our case, and they were also used for the restoration of white-light images to preserve equal conditions for all wavelengths. We must note that the white-light frames were slightly underrestored at spatial scales smaller than 0.″48 and therefore the photometric quantities should be used for comparison purposes only. This is not a drawback in the case of time series, where temporal changes are of prime concern.

From the registered and restored frames covering practically the whole field of view we extracted subfields of size 12″ × 12″ around the pores P1, P2, P3, P5, and P6, 20″ × 20″ around P4, and another 20″ × 20″ subfield contained a region of undisturbed photospheric granulation. In order to minimize seeing distortions, the subfields were destretched using modifications of routines written by Molowny-Horas & Yi (1994). The reference frames for destretching were determined individually for each image as averages of time subseries of five frames surrounding the image to be destretched. This enabled us to eliminate the seeing-induced shifts and preserve the real motions. After that we applied the k-ω filtering (subsonic) to remove acoustic waves and mainly the residual jitter induced by seeing. The cut-off phase velocity of the filter was set to 4 km s^{-1} (see Hirzberger et al. 1997 for discussion).

For a better identification of the facular points we subtracted, after a careful co-alignment, the white-light from the *G*-band images. After this, a threshold method was used to eliminate residual low-intensity fluctuations. Because of the small signal-to-noise ratio at high spatial frequencies in the *G*-band frames, we were able to detect reliably only large (>0.″6) *G*-band brightenings, corresponding presumably to large facular points or to concentrations of several small ones.

3.2. *Tracking Algorithms*

Because of the different characteristics of observed structures, we used different tracking algorithms that will be described briefly. To follow the evolution and proper motions of individual features we need to track them separately, recording their position, brightness, and size in each frame of the series (see Strous 1994; Strous et al. 1996). For large-scale motions an average flow map is sufficient. The tracking procedures were applied to data cubes composed of white-light images.

Small bright features (UDs in P4).—We used the feature-tracking technique developed by Sobotka et al. (1997a) and inspired by the previous work of Strous. In the first step we defined the umbral region using the isointensity level at $0.7I_{\rm phot}$ after 1.″5 × 1.″5 boxcar smoothing, and then we separated the UDs from the diffuse background by applying a simple image-segmentation method, based on an edge-enhancement algorithm: For each frame a differential image was computed by subtracting a smoothed image (boxcar 0.″43 × 0.″43) from the original one. From this differential image we computed a binary mask, setting pixel values higher than an empirically estimated threshold ($0.02I_{\rm phot}$) to 1 and the rest to 0. The original image was then multiplied by this mask, to produce a segmented image in which the bright peaks (UDs) conserved their original intensity, and the background was set to zero. In the second step the nonzero pixels forming an object (UD) were labeled by an object identification number which, together with the pixel coordinates, was stored in memory. After this object identification, in the third step, the spatial coincidences of objects in each pair of subsequent frames were investigated. Two objects were identified as predecessor/successor if they coincided in the coordinates of at least 1 pixel in both frames. Formation, death, splitting, merging, and temporary (shorter than 60 s) disappearance of objects due to seeing deterioration were taken into account (see Sobotka et al. 1997a for details). In the fourth step, to improve the reliability of the results, we excluded all objects with lifetimes shorter than four frames (60 s) or diameters smaller than 0.″25 or horizontal velocities larger than 1 km s^{-1} to avoid spurious relations between independent objects. From the procedure described above, we obtained the lifetimes of the objects (given by the number of frames in which the objects are present) and for each frame the magnitudes and positions of maximum intensities together with the effective diameters, derived from the number of pixels (area), of the objects. The average proper motion velocities of the features were calculated from their positions by means of least-squares linear fits (cf. Molowny-Horas 1994).

Granules and their fragments.—The tracking procedure applied to large bright features was analogous to the previous one in the first two steps. The only differences were that we did not isolate the umbral region and that the segmentation parameters, boxcar and threshold, were 0.″68 × 0.″68 and 0.025 $I_{\rm phot}$, respectively, to fit the typical sizes of the features. However, the tracking of objects in time was different. Since the intensity pattern of granules and their fragments developed in a very complex way, we preferred, instead of the automated tracking, to label the tracked objects manually in each frame to avoid confusion

due to multiple splitting and merging and to select the fragments that we were really interested in. From this procedure we obtained the lifetimes, and, for each frame, the magnitudes and positions of maximum intensities and the effective diameters. The instantaneous velocities of proper motions were calculated from the differences of the positions, smoothed previously by cubic splines.

Photospheric flows.—The standard method of local correlation tracking (LCT) (November & Simon 1988) was applied. We used the modifications of routines written by Molowny-Horas & Yi (1994). The FWHM of the Gaussian window used in the tracking was 0.″8. This characterizes the spatial resolution of the flow map. The time delay between correlated frames was 40 s. The flow maps were averaged over time to reduce measurement noise. The averaging times were equal to the total (85 or 67 minutes) and the half duration (42 or 33 minutes) of the time series. As a result we obtained the distribution of flows in the regions $12'' \times 12''$ around the pores P1, P2, P3, P5, and P6, and $20'' \times 20''$ around P4 and in the quiet granulation. Detailed flow maps of the region between P3 and P4 during temporary changes in intensity and flow patterns were computed with FWHM = 0.″6, time delay 20 s, and averaging time 10 minutes.

In order to check the reliability of the LCT routines we took one frame of the region around P5 and shifted it successively by 0.1, 0.3, 0.6, and 1 pixel in the x-, y-, and (x, y)-directions. Then we computed displacement maps for each couple of original-shifted frames under identical conditions as for flow maps. We obtained systematic errors of -25% (an underestimation by factor of 0.8) and standard deviations of random errors of $\pm 15\%$ in all cases. This is a plausible result since we do not pretend to very high accuracy in our transverse velocity measurements. We did not observe any irregularities of the displacements due to large intensity gradients at the edges of the pore. In addition to that, R. A. Shine (1998, private communication) recomputed the flow map of the region around P4 using his new LCT algorithm, and the result did not differ from that obtained by us.

4. TEMPORAL EVOLUTION OF FINE STRUCTURES IN THE LARGE PORE P4

4.1. *Spatial Distribution of Power of Intensity Variations*

The oscillatory region of the p-modes was filtered out as mentioned in § 3.1. Before the filtration was done, we inspected the k-ω diagram corresponding to the umbral region of the pore P4. The p-mode part of the diagram contained, together with the intrinsic p-modes, strong contributions from image jittering and deformations. The p-mode signal was very weak in our white-light data, as can be expected from the decrease of the p-mode amplitude with depth. In the following analysis we used the filtered data in all cases.

To obtain the general description of temporal changes in and around the pores we calculated the power spectra of temporal intensity fluctuations of $0.''25 \times 0.''25$ surface elements (cf. Sobotka, Brandt, & Simon 1995b). The constant and linear terms of the intensity variations were subtracted before the calculation. The power spectrum of each surface element was split into two frequency bands corresponding to characteristic periods of 6–30 minutes (slow changes) and 2–5 minutes (fast changes). The power was averaged over each frequency band. Then, for each band we constructed a two-dimensional surface map of the power. This represents something similar to a brightness-stability map of the observed region. Figure 2 shows the maps corresponding to the pore P4 in white light. We found the following:

1. The power in both frequency bands is enhanced in the vicinity of the pore boundary. On the other hand, large stretches of the boundary itself are not outlined by enhanced power, which means that the boundary remains stable during the observing interval. Rather, the enhancements of power correspond to the regions where the interaction pore–surrounding photosphere is favored. We shall see in § 5.2 that these enhancements are related to the locations and paths of inflow of bright features (small granules and granular fragments) from the surrounding photosphere.

2. In the 6–30 minute band the power is enhanced in some umbral regions rich in UDs. It reflects the temporal

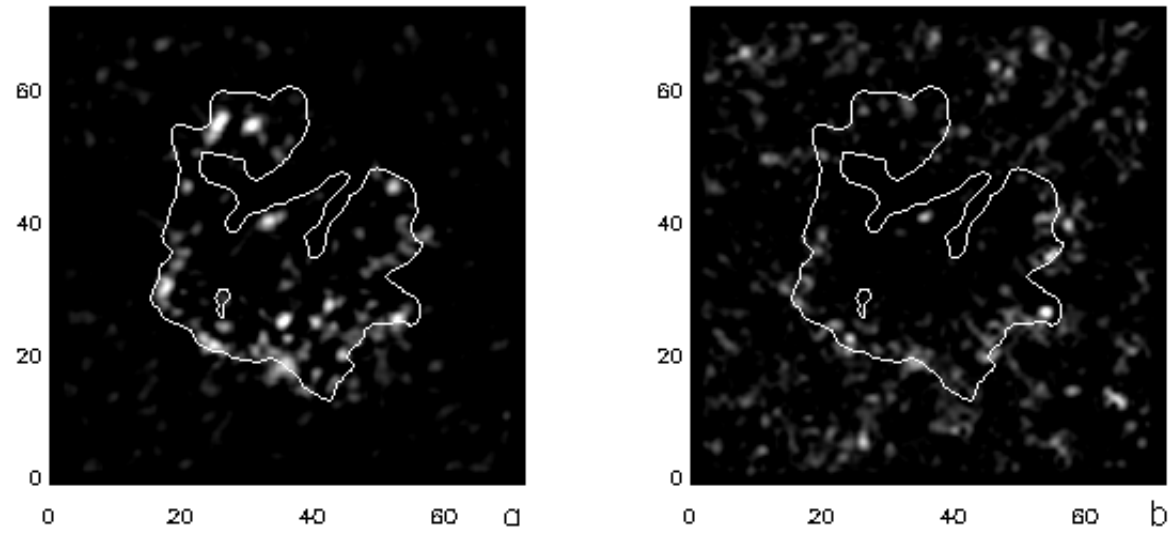

FIG. 2.—Surface maps of power of temporal intensity variations in and around the pore P4 in two frequency bands, corresponding to characteristic periods of (*a*) 6–30 and (*b*) 2–5 minutes. The gray-scale brightness increases with increasing power. The contour outlines the border of the pore derived from the time-averaged image of the series. The coordinate unit is 0.″25.

changes (formation, disappearance, motions, and intensity variations) of UDs. The power enhancement connected with the brightest cluster of UDs in P4, outlined by a contour in Figure 2 at coordinates (26, 28), is weak. We can conclude that this cluster is quite stable. The power corresponding to temporal changes of UDs in the 2–5 minute band is small compared with that in the 6–30 minute band.

3. No power enhancements are seen in light bridges; these structures are stable in intensity and shape.

4. The photospheric granulation shows many small regions with enhanced power, especially in the 2–5 minute band. They might be connected with the locations of convergent horizontal motions in the mesogranular flow pattern (see § 5.1 and compare Fig. 2*b* with Fig. 5).

4.2. *Evolution of Individual Bright Features in the Pore P4*

The maps of power of temporal intensity variations give us a hint as to which structures and regions should be studied in detail. An important topic is the evolution of individual bright features in the large pore P4.

4.2.1. *Light Bridges and Growing "Granule" inside the Pore*

Both light bridges present in P4 are practically without change in average brightness, shape, and size during the 67 minute time series. The intensity and area of the bridge on the left (see Fig. 1) are $(0.85–1.00)I_{\rm phot}$ and 6.53 arcsec^2; the corresponding values for the bridge on the right are $(0.78–0.95)I_{\rm phot}$ and 3.08 arcsec^2. The internal structure of both light bridges consists of small granules very similar to those forming strong light bridges in developed sunspots (cf. Sobotka et al. 1994). The temporal evolution of the internal structure is beyond the scope of this paper and will be analyzed elsewhere.

A large granule-like feature located in the upper left part of the pore P4 (marked as "G" in Fig. 1) increased its area steadily during the whole 67 minute time series. The feature was not a part of the light bridges. It maintained a constant mean intensity of $(0.89 \pm 0.02)I_{\rm phot}$ and its area, A, increased with a constant rate of 1.85 arcsec^2 hour^{-1} from 1.24 arcsec^2 at the beginning of the series to 3.42 arcsec^2 at the end. The corresponding effective diameter $d_{\rm eff} = \sqrt{4A/\pi}$ increased from 1.″3 to 2.″1. The growth of this "granule" was probably the first indication of the forthcoming decay of the pore.

4.2.2. *Umbral Dots*

We identified and tracked the evolution of 171 UDs that appeared during the 67 minute time series in the umbral region of P4. On average, about 41 UDs were seen in each frame and the filling factor (the ratio of the total area of the UDs to the umbral area of the pore) was 13%, i.e., 4% higher than in the umbra of a medium-size sunspot analyzed by Sobotka et al. (1997a).

Since the duration of the time series was relatively short, we were able to derive only the lower limits of the *lifetimes.* They ranged from 1 to 67 minutes; the average lifetime was 16 ± 14 minutes, and the median was 12 minutes. Two UDs were present during the whole series. To obtain a more realistic value of the average lifetime, we applied a simple statistical estimate, suggested by L. H. Strous (1998, private communication), which is not biased by the limited observation interval. The average number m of UDs visible in any given frame can be expressed as a product $m = b\bar{t}$ of the average birth rate b of UDs and their average lifetime $\bar{t}$. The average birth rate can be determined as $b = N/P$, where N is the number of all UDs that newly appeared during the whole observing interval P. Thus, $\bar{t} = m/b = mP/N$. If the numbers of UDs visible in individual frames show no temporal trend (which is our case), b and m are independent of P. During the interval $P = 66$ minutes, $N = 141$ new UDs appeared. These values together with $m = 41$ yield $\bar{t} = 19$ minutes. The histogram of lifetimes is shown in Figure 3*a*. In general, the number of UDs increases with decreasing lifetime in a similar way to that of the medium-size umbra (Sobotka et al. 1997a). The average and median lifetimes of the UDs in the pore are longer than those in the sunspot umbra (14 and 6 minutes, respectively). It seems that UDs are more stable in the relatively weak magnetic field of the pore (approximately 1000 G) than in strong field of developed umbrae.

The temporal *brightness* variation of UDs differed from one UD to another. There was no indication for a steep increase and slow decrease in intensity as pointed out by Adjabshirzadeh & Koutchmy (1980; cf. Denker 1998). In several cases, "bursts" or quasi-periodic variations of intensity with an average duration of 23 minutes were observed. Similar variations were also mentioned by Rimmele (1997) and by Sobotka et al. (1997b) for UDs in sunspot umbrae. The time-averaged brightnesses ranged between $0.47I_{\rm phot}$ and $0.96I_{\rm phot}$. The average value was 0.74 ± 0.10. The histogram is plotted in Figure 3*b*. There are two main differences with respect to the developed sunspot umbra. First, UDs are systematically brighter in the pore than in the umbra (typical brightnesses of 0.34 and 0.48 were reported by Sobotka et al. 1997b). This is related to the facts that the brightness of UDs is proportional to the intensity of the surrounding diffuse background (Sobotka et al. 1993) and that the minimum intensity in P4 ($0.34I_{\rm phot}$) is higher by a factor of 2 or more than that in the umbra. Second, the histogram of the time-averaged brightness of UDs in the pore has a single peak, while that constructed for the UDs in the sunspot umbra displayed two maxima (see Fig. 3 of Sobotka et al. 1997b). Bright UDs, corresponding to the secondary maximum, were concentrated at or near the umbra-penumbra boundary. In the pore P4, there is no difference between the spatial distributions of bright and faint UDs.

The histogram of the time-averaged *effective diameters*, $d_{\rm eff}$, is shown in Figure 3*c*. Its shape is analogous to the $d_{\rm eff}$ histogram of UDs in the sunspot umbra (see Fig. 3 in Sobotka et al. 1997a), that is, the number of UDs increases with decreasing $d_{\rm eff}$. The mean and median are $0.″32 \pm 0.″06$, and 0.″30, respectively. It should be noted that the values presented here correspond to the observed sizes, which are influenced by limited resolution of the telescope and image blurring. Moreover, the measurement of areas and sizes is dependent on the threshold level in the segmentation procedure, so that the numbers given here may differ systematically from the data obtained with other methods.

The *proper motions* of UDs are characterized by vectors of time-averaged velocities. The accuracy of the velocity determination of individual UDs increases with lifetime—the standard deviation is approximately 0.1 km s^{-1} for UDs with lifetimes less than 10 minutes, but 0.02 km s^{-1} for lifetimes greater than 10 minutes. Thus, in addition to the histogram of velocity magnitudes, v, of the whole sample, we calculated another one including 97 UDs with lifetimes

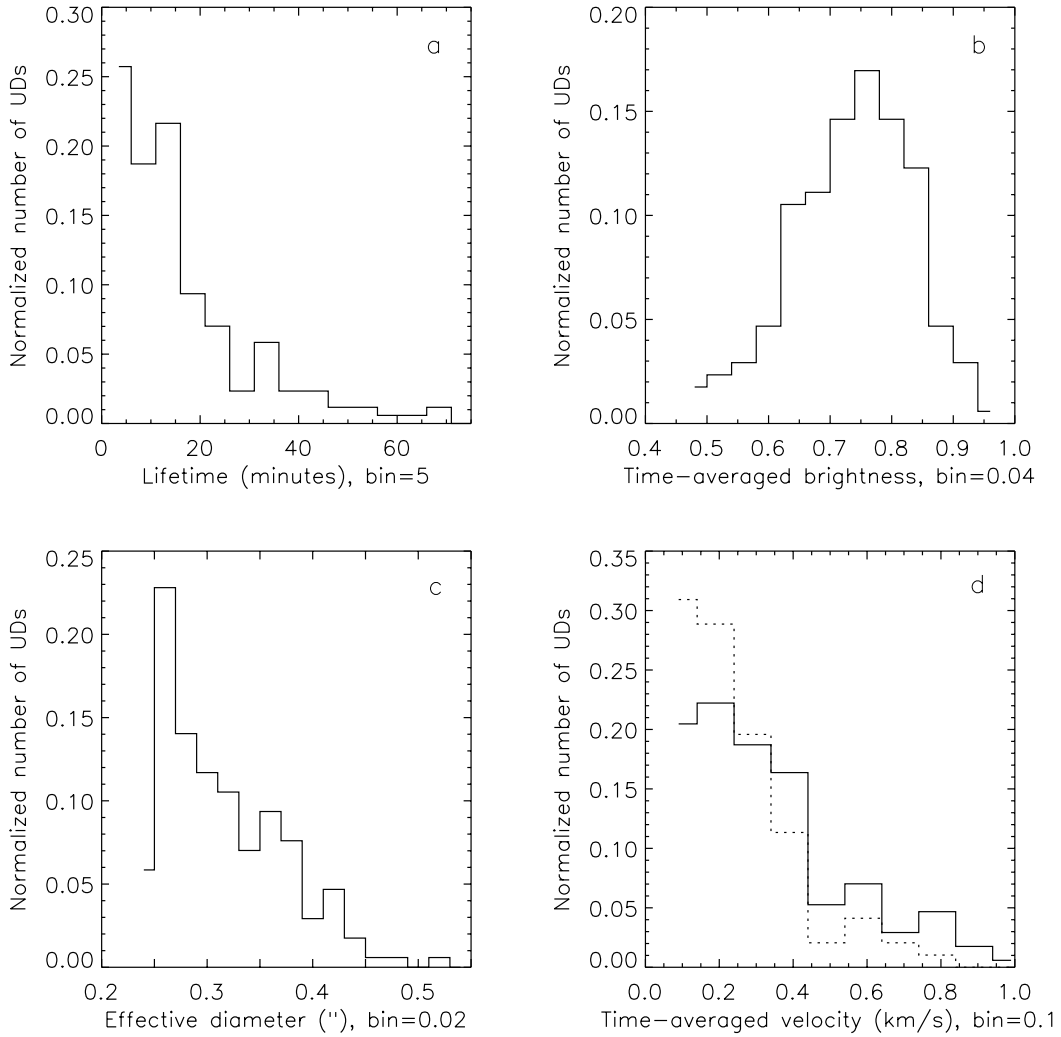

FIG. 3.—Histograms of time-averaged parameters of 171 UDs in the pore P4: (*a*) lifetimes, (*b*) brightnesses in units of $I_{\rm phot}$, (*c*) effective diameters, and (*d*) magnitudes of proper-motion velocities for all 171 UDs (*solid line*) and for 97 UDs with lifetimes greater than 10 minutes (*dotted line*).

longer than 10 minutes. Both histograms are plotted in Figure 3*d*. The number of UDs increases with decreasing v. The average and median values of v for the whole sample are 0.32 ± 0.21 km s^{-1} and 0.26 km s^{-1}, respectively. About half of UDs with lifetimes greater than 10 minutes move more slowly than 0.2 km s^{-1}. The motions of the UDs faster than 0.2 km s^{-1} are directed mostly inward toward the pore. In general, the distribution of the velocity vectors is similar to that in the sunspot umbra (Fig. 8 in Sobotka et al. 1997b) and means that fast and slow UDs can be found at any location in the pore.

5. CONVECTIVE STRUCTURES AROUND THE PORES

5.1. *Mesogranular Pattern and Bright Network Points*

LCT techniques (§ 3.2) were employed to study the horizontal motions of intensity features in and around the pores. The spatial resolution of the tracking (0.″8) was high enough to detect motions of small granules, granular fragments, and collective motions inside the pores.

In all flow maps we see the typical "rosetta" velocity patterns characteristic of mesogranulation (November et al. 1981; November 1989). These patterns are practically independent of adopted averaging times (total or half duration of the series), and they survive coherently over the entire period of observation (85 or 67 minutes), since the lifetime of mesogranules is about 3 hours (Muller et al. 1992). The nearest neighbor (center-to-center) distance of the rosettas in the $20'' \times 20''$ region of quiet granulation is 4.″1 on average. The largest velocities in the granular flow field are on the order of 1 km s^{-1}, and the spatial average is 0.4 km s^{-1}, in accordance with previous measurements made by Title et al. (1989), Simon et al. (1994), and Strous et al. (1996). Averaging all the frames of the time series, we obtain an image that still shows intensity fluctuations on granular length scales. Some bright and dark areas in this average image are spatially correlated with the centers of rosettas (with diverging flows) and the locations of converging flows, respectively. The correlation coefficient between the divergence values and brightnesses in the average image is 0.52. It was proved by November (1994) that the flow divergence corresponds to updrafts and the flow convergence (negative divergence) to downdrafts in the photosphere. The bright areas in the average image reflect the presence of bright, long-lived and rapidly expanding granules at the updrafts (Brandt et al. 1991), and the dark areas correspond to the locations of short-lived and less intense granules at the downdrafts.

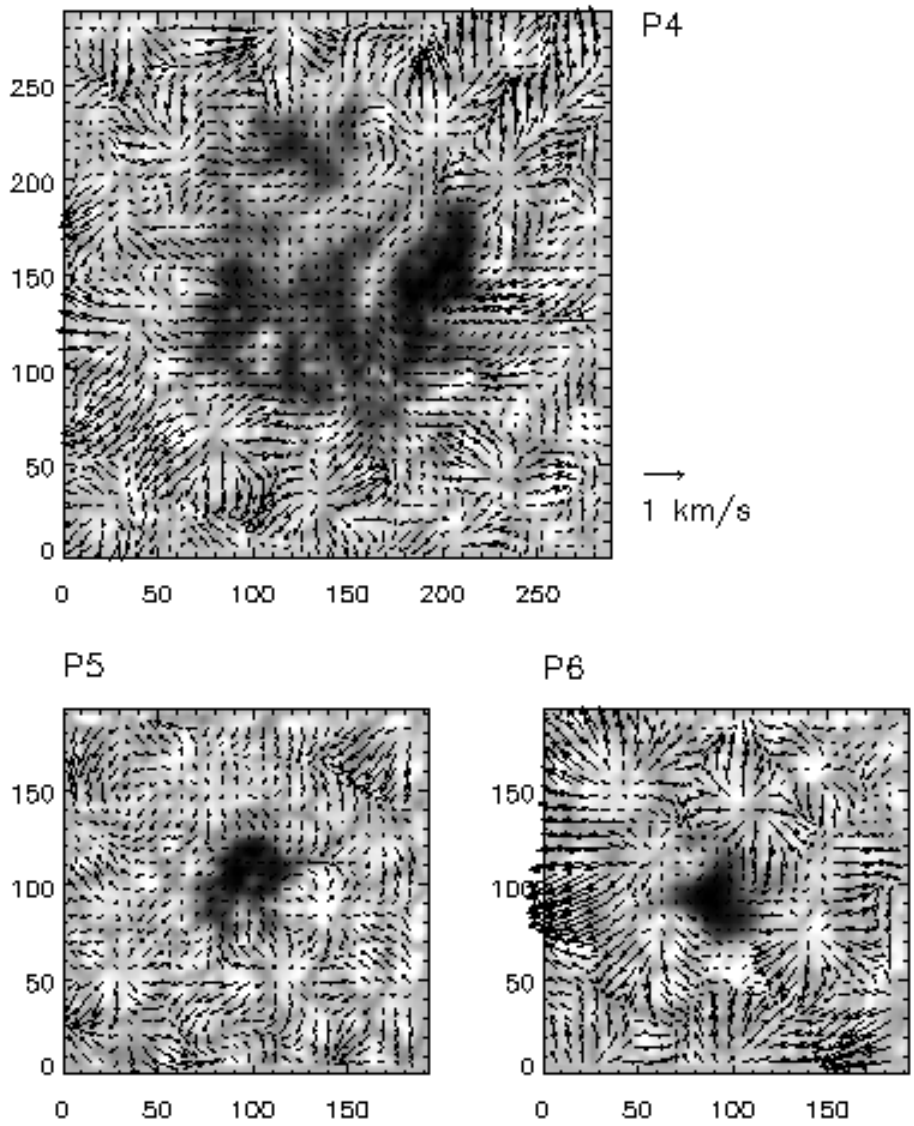

FIG. 4.—Flow maps of regions containing the pores P4, P5, and P6. Maximum velocities are between 0.8 and 1.1 km s^{-1}. Underlying white-light frames are from the middle of the time series. The coordinate unit is 1 pixel, i.e., 0.″062.

The examples of flow maps for pores P4, P5, and P6 superposed on white-light frames are displayed in Figure 4. The flow maps for P1, P2, and P3 show analogous behavior. The maximum velocities are between 0.8 and 1.1 km s^{-1}, and the spatial average is 0.3–0.4 km s^{-1}, that is, the velocity magnitudes are similar to those in quiet granulation. The velocities of umbral features inside P4 are 0.2 km s^{-1} (maximum) and 0.1 km s^{-1} (spatial average). They are consistent with the velocities obtained using the object-tracking algorithm, if we take into account the spatial resolution of the LCT (0.″8).

The emergence of small pores with diameters $\leq 3''$ seems to distort the mesogranular structure only slightly. The mean nearest neighbor distance of 4″ between the centers of rosettas located around the pore is almost equal to that in quiet granulation. The situation is different in case of P4 (diameter 8.″9). The large pore reorganizes the mesogranular flow pattern, pushing the rosettas away from each other and making them encircle the pore boundary. The mean nearest neighbor distance between the centers of rosettas around the perimeter of P4 is 5.″1.

Motions of granules in the vicinity of pores are driven by mesogranular flows. Motions toward the pore dominate in a zone out to a distance of 2″ from the pore's border. The centers of rosettas are mostly located at this distance. They form a ringlike structure with positive divergence, clearly seen in the gray-scale divergence maps displayed in Figure 5. At larger distances the granules move away from the pore. When a pore converts to a sunspot and the penumbra is formed, this structure disappears and is substituted by the outward motions along the dark filaments in the outer penumbra (Zirin & Wang 1989; Shine et al. 1994), outward motions of granules near the penumbral border (Muller & Mena 1987; Shine et al. 1987), and by the inward motions of penumbral grains (Muller 1973).

The *G*-band brightenings (clusters of facular points) observed around the pores P3–P6, have lifetimes ranging from 20 to more than 67 minutes (length of the series). They appear recurrently at locations that surround the pores and that are related to the mesogranular flow pattern. The *G*-band brightenings are mostly located at the downdrafts, areas with negatively divergent horizontal motions. This is

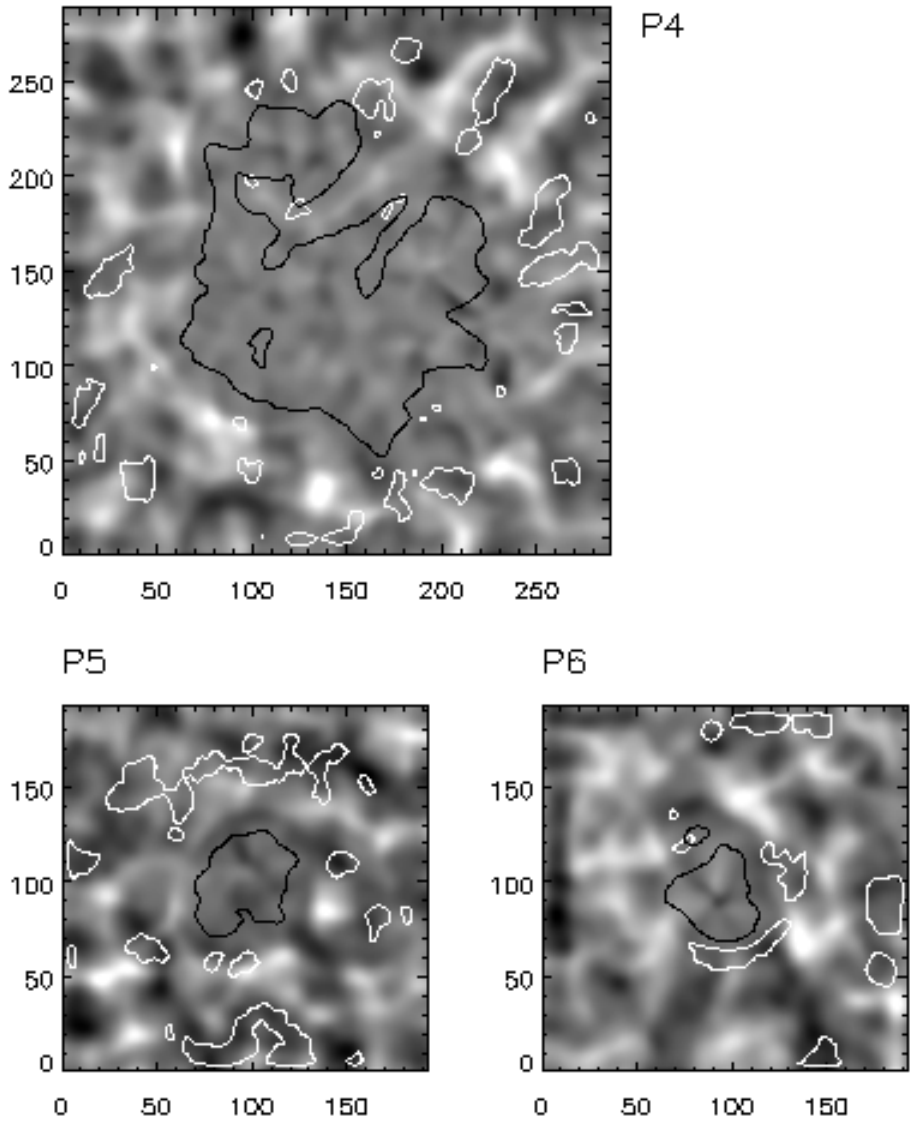

FIG. 5.—Time-averaged positions of brightenings in the *G* band (*white contours*) superposed to the gray-scale maps of divergence (white is for positive divergence, and black is for negative divergence). Black contours outline the borders of the pores. The regions and coordinate units are as in Fig. 4.

demonstrated in Figure 5, where the time-averaged positions of *G*-band brightenings, outlined by white contours, overlay the divergence maps of the regions around P4, P5, and P6. If we assume that the *G*-band brightenings represent magnetic field concentrations (see, however, Title & Berger 1996 and Topka, Tarbell, & Title 1997), the flux tubes are concentrated in the downdrafts by the horizontal motions of the meso- and supergranulation (Yi & Engvold 1993).

5.2. *Interaction of Surrounding Granules with the Pores*

In the previous section we mentioned the 2″ zone around the pores where the motions toward the pore dominate. These motions, as seen in the movie of P4, sometimes result in a penetration of bright features from the photosphere into the pore. Two morphological types of this effect can be observed: (1) small granules located at the pore border that shrink, separate from the edge, and move inward and (2) large granules that, instead of shrinking, split into several pieces. The fragments located close to the border then move into the pore. Once penetrated inside, the fragments or shrunk granules cannot be distinguished from UDs. They continue to move inward, and their brightness and size decrease until they disappear. The examples of both types are shown in a series of frames displayed in Figure 6. The penetrations occur around the whole perimeter of the pore. They are often accompanied by the presence of elongated bright features located near the pore's edge (see frame 8 in Fig. 6), which may indicate a local tilt in the magnetic field.

Using the method described in § 3.2, we tracked the evolution and proper motions of 14 randomly selected bright granules and fragments that penetrated into the pore P4. Their trajectories are plotted in Figure 7. They are located in the areas with enhanced power of temporal intensity variations, particularly in the 2–5 minute band (see Fig. 2). The beginning of penetration is defined as the moment when the feature becomes completely separated from the pore border; the end of penetration is defined as the moment when the feature is observed for the last time before it disappears. The duration of penetration ranges from 3 to 14 minutes, and its mean value is 6.4 minutes. The depth of penetration, i.e., the distance between the positions

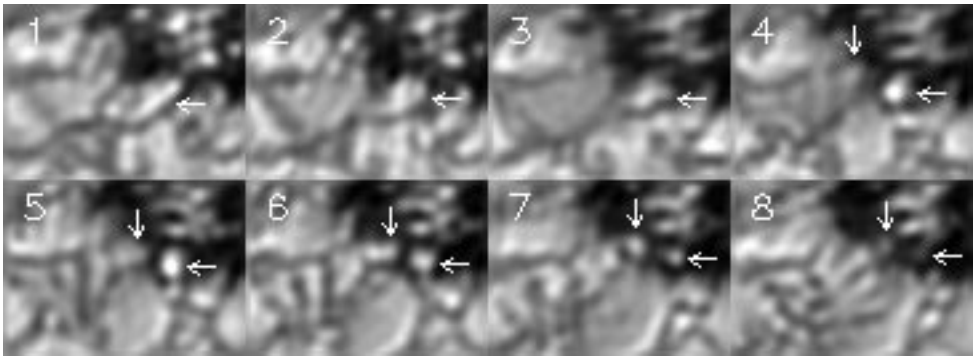

FIG. 6.—Sequence of frames (5″.6 × 4″.1), separated in time by 2 minutes, showing (1) the transition from a photospheric granule, located at the border of P4 and marked by the horizontal arrow, to a UD, and (2) the fragmentation of another granule followed by the penetration of its innermost fragment, marked by the vertical arrow, into P4. Note the elongated structures at the pore border in the center of frame 8.

at the beginning and at the end of penetration, is relatively small—0″.4 on average—and the maximum observed depth of penetration is 1″. The velocities of proper motions, averaged over the whole period when the feature is observed, are in the range 0.56–1.82 km s^{-1}. They are anticorrelated with the duration of penetration. For comparison, the average speed of penumbral grains moving toward the umbra is smaller by factor of 2–3.

The tracking method enabled us to determine the temporal variations of brightnesses, effective diameters, and instantaneous velocities of penetrating features. The brightnesses before and at the beginning of penetration are higher than the mean intensity of the undisturbed photosphere, and they decrease during the penetration. The effective diameters at the beginning of tracking are in a broad range of 0″.4–1″ (depending on whether we are observing a shrinking granule or a granular fragment) and decrease with small fluctuations during the whole tracking period. The instant-

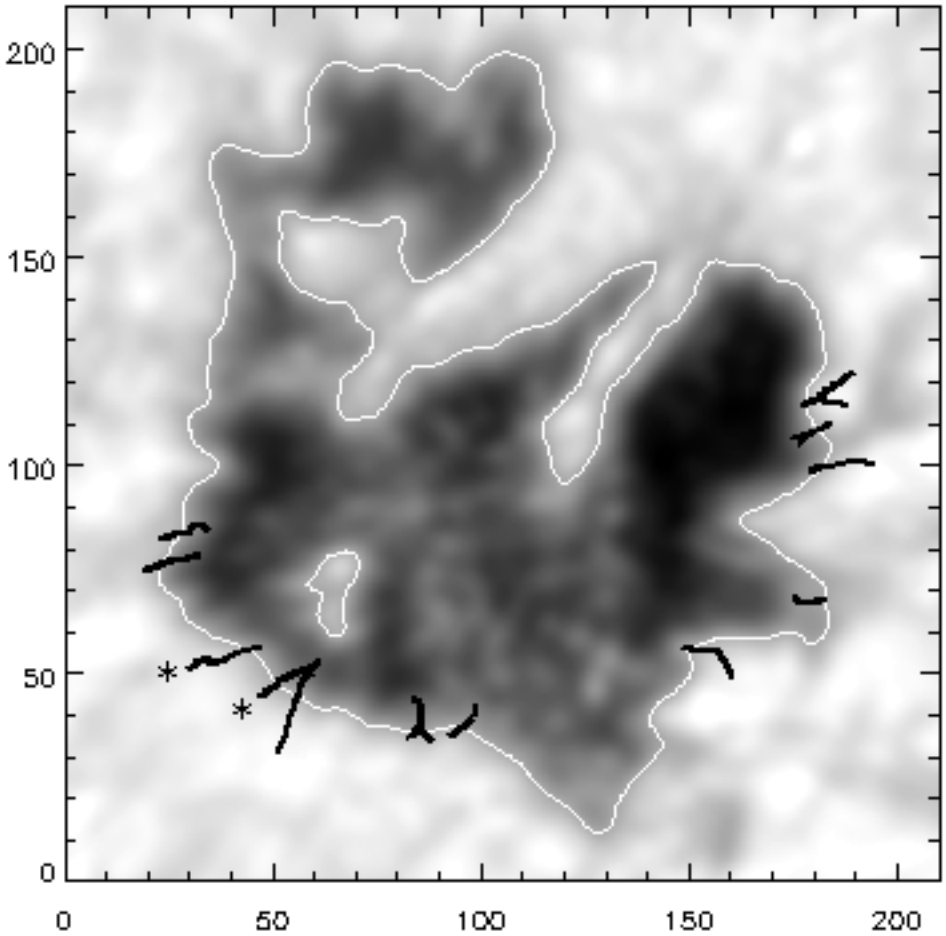

FIG. 7.—Trajectories of 14 bright features penetrating into the pore P4, plotted over the time-averaged image of the series. The white contour corresponds to the intensity of $0.83 I_{phot}$. The coordinate unit is 1 pixel, i.e., 0″.062. The trajectories of features shown in Fig. 6 are marked by asterisks.

aneous velocities before penetration show a large scatter from 0.7 to 3.0 km s^{-1}. There is no clear trend in their temporal variations, but in 70% of cases we observe a deceleration at the beginning and end of penetration. In Table 2 we present the average values of these parameters for the sample of 14 features (before, at the beginning, and at the end of penetration) together with the standard deviations that characterize the scatter of individual values.

6. CHANGES IN INTENSITY AND FLOW PATTERNS DUE TO MAGNETIC FIELD

6.1. *Formation of a Transitory Penumbra?*

The bright region intruding into the darkest part of the pore P4 (labeled as F in Fig. 1) differs in its morphology and kinematics from the areas described in the previous section. A phenomenon, looking like the formation of a transitory penumbra, started in this region soon after the beginning of the observation and existed for about 40 minutes.

At the beginning of the time series the region was formed by a bright photospheric granule (effective diameter 1″.2, maximum brightness $1.05I_{\rm phot}$) extending into the pore. The phenomenon started (time $t = 0$) with the onset of a strong and organized flow from the photospheric area behind the granule toward the pore. The duration of this inflow, displayed in the left part of Figure 8, was 10 minutes. The average and maximum speeds, measured with the LCT algorithm, were 1.5 and 2 km s^{-1}, respectively, i.e., higher by a factor of 2–3 than the usual flow speed around the pore.

At $t = 4$ minutes the granule split into elongated fragments, and at $t = 10$ minutes it was replaced by a highly dynamical filamentary structure oriented perpendicularly to the pore edge. The bright filaments appeared as small elongated features and increased their length by expansion at both ends with velocities of 1.3 km s^{-1} directed toward the pore and of 2 km s^{-1} out from the pore. After 6–9 minutes the filaments reached the maximum length of about 2″.7 and decayed, being replaced at locations similar to the previous ones. Two or three bright filaments were always present at the same time. Their width was 0″.3–0″.5, with a maximum brightness $(0.95–1.05)I_{\rm phot}$, and the minimum brightness of dark spaces between them was 0.79. The duration of this evolutionary phase was 22 minutes.

TABLE 2

AVERAGE VALUES FOR 14 BRIGHT FEATURES PENETRATING INTO THE PORE P4

Parameter	Before Penetration	Beginning of Penetration	End of Penetration
Brightness ($I_{\rm phot}$)	1.14 ± 0.09	1.08 ± 0.09	0.73 ± 0.08
Effective diameter (arcsec).....	0.69 ± 0.18	0.58 ± 0.10	0.31 ± 0.06
Velocity (km s^{-1})	2.0 ± 0.7	1.6 ± 0.6	0.7 ± 0.4

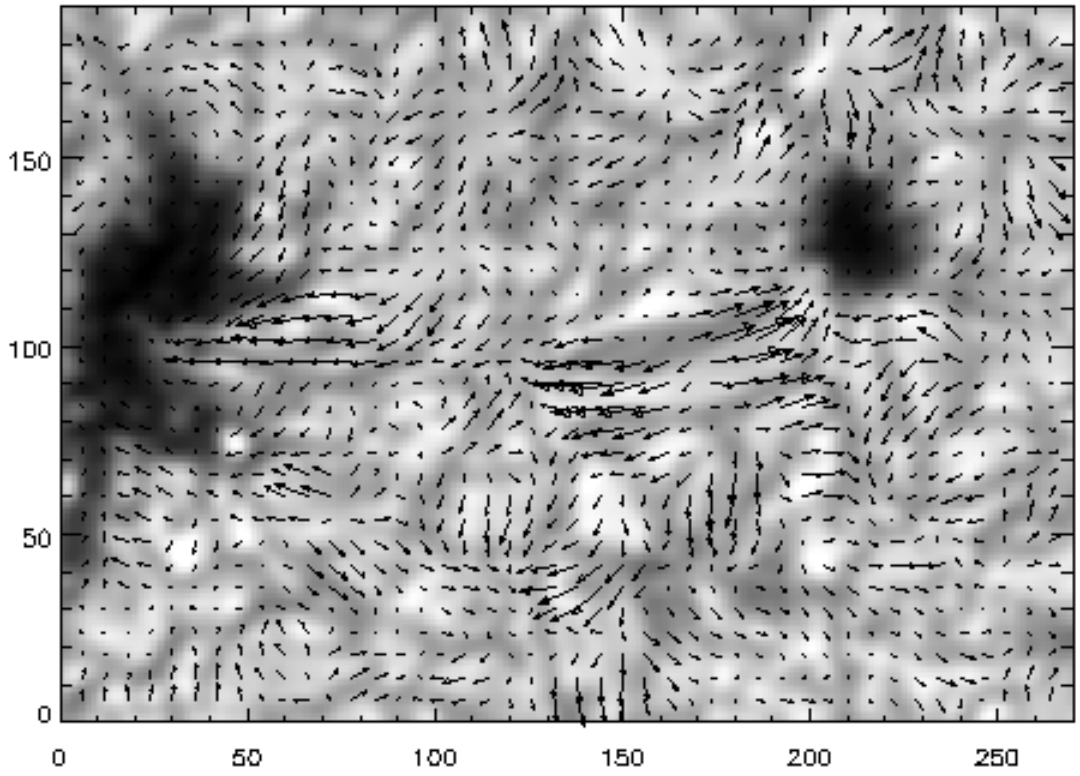

FIG. 8.—Flow map showing (1) the strong organized motion (maximum speed 2 km s^{-1}) directed toward the region of the pore P4 where the penumbra-like filamentary structure was formed (*left*) and (2) the motions (maximum speed 3 km s^{-1}) connected with the transient changes in the granular pattern in the region between the pores P4 and P3 (*right*). The underlying white-light frame shows the field with P3 (*right*) and a part of P4 (*left*) at $t = 10$ minutes after the start of the motions. The coordinate unit is 1 pixel, i.e., 0″.062.

After $t = 32$ minutes the formation of filaments ceased and the structure decayed to randomly oriented fragments. At $t = 42$ minutes a new photospheric granule (effective diameter 1".2, maximum brightness $1.13I_{\rm phot}$) was established.

The phenomenon described above does not represent the typical process of penumbra formation. Neither inward-moving penumbral grains nor outward motions in the dark spaces, typical for developed penumbrae, were observed. However, the filamentary structure is a manifestation of magnetic field strongly inclined with respect to the normal. Moreover, no brightenings were observed in the *G* band, which can also be a consequence of predominantly horizontal magnetic fields. Since the filamentary structure appeared immediately after the strong horizontal flow from the neighboring photosphere toward the pore, we can suspect a casual relationship between these two phenomena.

6.2. *Transient Changes of Granular Pattern between Pores P3 and P4*

Simultaneously with the transitory "penumbra" formation at the border of P4, another interesting phenomenon occurred in the region between the "penumbra" location and pore P3. Figure 9 shows four selected frames of this process. One minute before the onset of the strong flow into P4, mentioned in the previous section and adopted as $t = 0$, an elongated granule (labeled G1 in Fig. 9) emerged from a large intergranular space and increased its length and brightness rapidly. It was followed by a second elongated granule (G2), formed at $t = 3$ minutes. The ends of both granules expanded with velocities of 2.7 km s^{-1} toward P4 and of 3.0 km s^{-1} toward P3. The granules were separated by a dark filament with maximum length of 3".8 $\equiv$ 2800 km (approximately) and minimum brightness of $0.81I_{\rm phot}$ at $t = 10$ minutes (Tarbell et al. 1990 found that dark alignments seen in the continuum were typically 1500 to 4000 km long). At $t = 18$ minutes both granules reached their maximum brightness of $1.25I_{\rm phot}$, and they continued to expand with velocities of 1.7 km s^{-1} (toward P4) and 2.6 km s^{-1} (toward P3). At $t = 30$ minutes the granules started to decay, and at $t = 34$ minutes they disappeared. After that, usual intensity and motion structures corresponding to undisturbed granulation were reestablished. The total duration of the event was 35 minutes, affecting an area of 6 arcsec^2 with a maximum length of 3".8.

As commented at the end of § 5.1, most of the clusters of bright facular points, observed in the *G* band, were stationary, coinciding spatially with the downdrafts of mesogranular flows. However, close to the ends of expanding elongated granules G1 and G2 appeared two strong

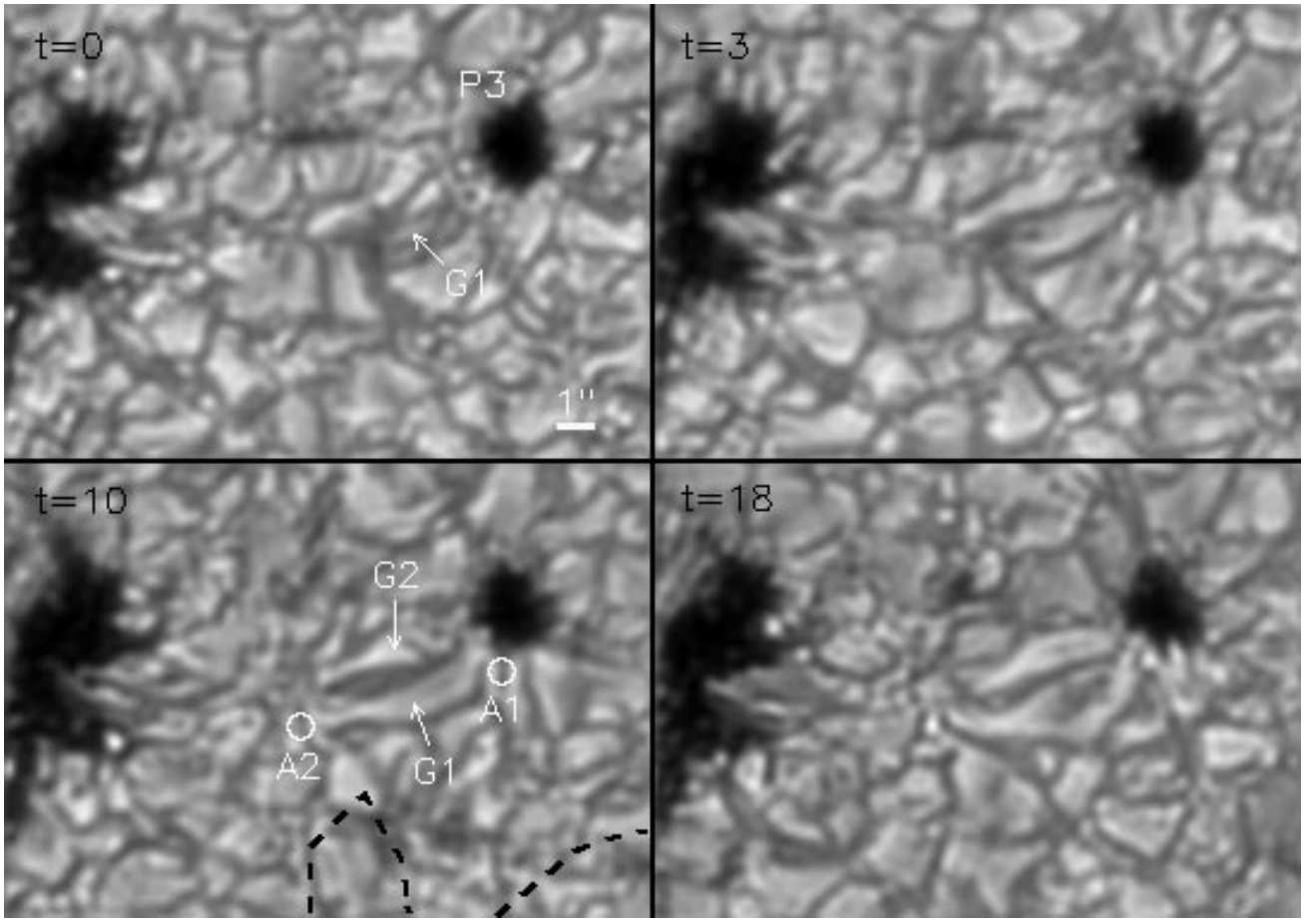

FIG. 9.—Selected frames displaying the transient changes of granular pattern between the pores P4 and P3. Note also the formation of the penumbra-like filamentary structure at the border of P4. Expanding elongated granules are marked as G1 and G2. The circles labeled A1, A2 show the locations of moving *G*-band brightenings. The dashed line represents the boundary between the opposite magnetic polarities. The field of view is as in Fig. 8. Time, *t*, is measured in minutes from the beginning of the event (see text and caption of Fig. 8).

enhancements in the *G*-band brightness (A1, A2; see Fig. 9), moving away from each other. As observed in the *G*-band differential images, A1 and A2 were formed at $t = 2$ and $t = 6$ minutes, respectively. A1 moved toward P3 with a speed of 0.6 km s^{-1} and A2 toward P4 with 0.8 km s^{-1}. These velocities were similar to those observed in facular points (0.61 km s^{-1}) by Strous et al. (1996). A1 and A2 disappeared at the same moment, $t = 36$ minutes, 2 minutes after the decay of G1 and G2 in white light.

The transient reconfiguration of the granular pattern into expanding elongated granules, separated by long dark filaments, is a strong indication of the emergence (or local formation) of a nearly horizontal magnetic field. Following van Driel-Gesztelyi & Petrovay (1990), the different expansion speed of granular borders can be interpreted as a consequence of the tilt in the emerging magnetic field. The moving *G*-band brightenings A1, A2 may coincide with the footpoints of the field.

Since the formation of the penumbra-like filamentary structure at the border of P4 and the reconfiguration of granular pattern in the photospheric region between P4 and P3 was observed at the same time, we can expect that a common physical process is behind these two events. The magnetic polarity of pore P3 was equal to that of P4. However, the measurements obtained with the Ondřejov Observatory magnetograph 20 minutes after the events (V. Bumba & M. Klvaňa 1998, private communication) have shown that the neutral line between magnetic polarities was located close to the region where the events took place (see Fig. 9; for the role of neutral lines in magnetic flux emergence see Strous 1994). Thus, a possible explanation of these events might be that a temporary intrusion of the opposite magnetic polarity into the region between P3 and P4 gave rise to a transient system of magnetic field lines that were nearly horizontal and connected the intrusion with the strongest local magnetic concentrations—the pores. The "penumbra" formation and the granule reorganization occurred when this horizontal magnetic field emerged through the photospheric layer. The expanding elongated granules and dark alignments were observed earlier by Wang & Zirin (1992) in a young active region.

7. DISCUSSION AND CONCLUSIONS

Time series of high-resolution white-light and *G*-band images were used to study temporal changes and evolution of fine structures in and around solar pores. The most important results are summarized as follows:

1. Two-dimensional maps of the integrated power of temporal intensity variations are a suitable tool giving an overview of the regions where the interaction pore-surrounding photosphere takes place and of the variability of fine structures inside the pore at different timescales.

2. Parameters of UDs (lifetime, brightness, size, and proper motion) in the large ($D = 8''.9$) pore P4 are similar to those in the umbrae of developed sunspots, except that the UDs in the pore live longer, are brighter, and have a higher filling factor than UDs in the medium-size umbra described by Sobotka et al. (1997a, 1997b). This is probably due to a weaker magnetic field ($\simeq 1000$ G) in the pore.

3. Motions of granules in the vicinity of pores are driven by mesogranular flows. The centers of positive divergence are mostly located at distances of 2″ from the pore border, forming a ringlike structure. As a consequence, motions toward the pore dominate in the 2″ zone around the pore boundary, while at larger distances the granules move away from the pore. Small pores have only a small influence on the mesogranular flow pattern. The large pore, P4, however, reorganizes the flows, pushing away the centers of positive divergence and making them encircle the pore boundary at the distance of 2″.

4. Small granules and granular fragments located close to the pore border sometimes penetrate into the pore, where they get smaller and move inward as short-lived (6.4 minutes on average) UD-like features. The average depth of penetration is small (0″.4). This process is often accompanied by the presence of elongated small-scale structures in the photosphere close to the pore boundary, which may indicate a local tilt in the magnetic field.

5. Two phenomena of temporary reconfiguration of the intensity pattern, accompanied by strong horizontal motions of 2–3 km s^{-1}, were observed. The first consisted in the formation of a penumbra-like structure at the border of the large pore, P4, the second in the transformation of the granular field between P4 and the adjacent pore, P3, to a system of expanding elongated granules separated by dark filaments. Both phenomena took place near each other, parallel in time, and their duration was about 35 minutes. They can be explained as a consequence of emerging bipolar magnetic "loops" caused by a temporary protrusion of opposite magnetic polarity.

The interpretation of these results is constrained by the fact that we observe only the layer where the continuum radiation is formed ($\tau = 1$). However, in the absence of three-dimensional spectropolarimetric observations at appropriate temporal and spatial resolution, we can suggest some ideas about the interaction between the quasi-vertical magnetic field of pores and the surrounding convective cells.

We have no doubt that granules and their fragments located near the pore border move toward it, as reported already by Wang & Zirin (1992). The detection of motions with the LCT technique depends strongly on the size of the tracking window. Denker (1998) used images with excellent resolution, but his tracking window of 2″ was too large to detect the narrow zone where these inward motions took place.

Small granules and granular fragments, coming from nonmagnetic regions, are often able to cross the boundary with the magnetic medium—the pore. At the same time, in the regions of penetration, elongated small-scale structures indicate a local inclination of magnetic field at the pore border. The main question to be solved in this context is a typical chicken-and-egg dilemma. Which comes first, (1) regions of inclined magnetic field, where an easier way for the penetration of hot plasma blobs is offered, or (2) regions where fast-moving convective elements, pushed by mesogranular motions oriented toward the pore, collide with the boundary, producing a local instability of the field and favoring this way the penetration of the hot bubble into the pore? In other words, does the entrance of the hot plasma element take place along the lines of force in a preexisting, tilted field, or simply by pulling aside the vertical field lines of the umbral wall? This topic will be elaborated on in a separate theoretical paper. Nevertheless, the result of both scenarios is that a UD-like feature is captured into the pore.

P4 was an excellent example of a short-lived pore, and we observed it when the maximum development phase passed to the decay. Different processes were proposed to explain

the decay of sunspots. Simon & Leighton (1964) first proposed that sunspot decay may be produced by the "gnawing" action of supergranular motions at the edges of the sunspot. Recently, Petrovay & Moreno Insertis (1997) developed a model of sunspot decay, called turbulent erosion, based on the action of small-scale adjacent granular motions, which reproduced the observed parabolic decay law (Petrovay & van Driel-Gesztelyi 1997). We believe that the observed capture of hot plasma blobs by the pore P4 constitute the microscale manifestation of turbulent erosion, based on the action of all the known spatial scales of photospheric convection (granulation, mesogranulation, and supergranulation). It has already been suggested by Zwaan (1992) that sunspots with a high filling factor of bright structures decay faster than compact dark spots. The granular penetration events are induced by velocity flows hitting the pore (sunspot) boundaries. It is well known that sunspots become stable when they form a moat around them (Vrabec 1974; Brickhouse & Labonte 1988). The pore P4 presumably was not able to develop such a barrier and was destroyed by the action of the surrounding convective motions.

Formation of the penumbra is one of the stabilizing processes in sunspot evolution. Very often, penumbral filaments appear first on the side that is oriented outward from the active region. The appearance of the filamentary penumbra-like structure at the edge of P4 facing toward the temporary intrusion of the magnetic neutral line and to another pore, P3, was not such a case. Recently, Leka & Skumanich (1998) also observed that a sector of pore penumbra was initially formed close to the neutral line. They suggested that the penumbral magnetic field could result from emerging flux that became "trapped" as penumbra rather than continuing to emerge and turn vertical. Their scenario, in principle, corresponds to the phenomenon that we have observed. However, the magnetic field of P4 was too weak to "trap" the emerging flux and to create a stable penumbral sector. The rapid disintegration of the pore did not allow a definitive formation of the penumbra.

We are grateful to D. Kennerdahl and G. Hosinsky for their support during the observations. J. W. Harvey kindly supplied the NSO/Kitt Peak magnetograms, produced in cooperation with NSF/NOAO, NASA/GSFC, and NOAA/SEL. We appreciate the comments of an anonymous referee who contributed to the improvement of this paper. T. Mahoney revised the English text. The sunspot tracker was developed and built by the ETH Zürich astronomy group under the leadership of C. Keller. The Swedish Vacuum Solar Telescope is operated on the island of La Palma by the Royal Swedish Academy of Sciences at the Spanish Observatorio del Roque de los Muchachos of the Instituto de Astrofísica de Canarias. This work was partially financed by the Spanish DGES project 95-0028 and by the Key Project K1-003-601 of the Czech Academy of Sciences. A. H. gratefully acknowledges the support by the Austrian Fonds zur Förderung der Wissenschaftlichen Forschung (Project 10748), and M. S. gratefully acknowledges grant 205/97/0500 by the Grant Agency of the Czech Republic.

REFERENCES

Adjabshirzadeh, A., & Koutchmy, S. 1980, A&A, 89, 88
Beckers, J. M., & Schröter, E. H. 1968, Sol. Phys., 4, 303
Bonet, J. A., Sobotka, M., & Vázquez, M. 1995, A&A, 296, 241
Brandt, P. N., Ferguson, S., Scharmer, G. B., Shine, R. A., Tarbell, T. D., Title, A. M., & Topka, K. 1991, A&A, 241, 219
Brants J. J., & Steenbeek, J. C. M. 1985, Sol. Phys., 96, 229
Bray, R. J., & Loughhead, R. E. 1964, Sunspots (London: Chapman & Hall)
Brickhouse, N. S., & Labonte, B. J. 1988, Sol. Phys., 115, 43
Bumba, V., & Suda, J. 1984, BAIC, 35, 28
Collados, M., del Toro Iniesta, J. C., & Vázquez, M. 1987, Sol. Phys., 112, 281
Collados, M., Martínez Pillet, V., Ruiz Cobo, B., del Toro Iniesta, J. C., & Vázquez, M. 1994, A&A, 291, 622
Collados, M., & Vázquez, M. 1987, A&A, 180, 223
Denker, C. 1998, Sol. Phys., 180, 81
Ewell, M. W. 1992, Sol. Phys., 137, 215
Hirzberger, J., Vázquez, M., Bonet, J. A., Hanslmeier, A., & Sobotka, M. 1997, ApJ, 480, 406
Jahn, K. 1997, in ASP Conf. Ser. 118, First Advances in Solar Physics Euroconference: Advances in the Physics of Sunspots, ed. B. Schmieder, J. C. del Toro Iniesta, & M. Vázquez (San Francisco: ASP), 122
Keppens, R., & Martínez Pillet, V. 1996, A&A, 316, 229
Kitai, R. 1986, Sol. Phys., 104, 287
Klvaňa, M., & Bumba, V. 1994, in ESO Conference and Workshop Proc. 50, Handling and Archiving Data from Ground-based Telescopes, ed. M. Albrecht & F. Pasian (Garching: ESO), 173
Kopp, G., & Rabin, D. 1992, Sol. Phys., 141, 253
Kusoffsky, U., & Lundstedt, H. 1986, A&A, 160, 51
Leka, K. D., & Skumanich, A. 1998, ApJ, 507, 454
Martínez Pillet, V. 1997, in ASP Conf. Ser. 118, First Advances in Solar Physics Euroconference: Advances in the Physics of Sunspots, ed. B. Schmieder, J. C. del Toro Iniesta, & M. Vázquez (San Francisco: ASP), 212
Miller, R. A. 1960, J. British Astron. Assoc., 70, 100
Molowny-Horas, R. 1994, Sol. Phys., 154, 29
Molowny-Horas, R., & Yi, Z. 1994, ITA (Oslo) Internal Report No. 31
Muglach, K., Solanki, S. K., & Livingston, W. C. 1994, in Solar Surface Magnetism, ed. R. J. Rutten & C. J. Schrijver (Dordrecht: Kluwer), 127
Mullan, D. J. 1983, in Activity in Red-Dwarf Stars, ed. P. B. Byrne & M. Rodono (Dordrecht: Reidel), 527
Muller, R. 1973, Sol. Phys., 29, 55
———. 1976, Sol. Phys., 48, 101
Muller, R. 1992, in Sunspots: Theory and Observations, ed. J. H. Thomas & N. O. Weiss (Dordrecht: Kluwer), 175
Muller, R., Auffret, H., Roudier, T., Vigneau, J., Simon, G. W., Frank, Z., Shine, R. A., & Title, A. M. 1992, Nature, 356, 322
Muller R., & Mena, V. 1987, Sol. Phys., 112, 295
November, L. J. 1989, ApJ, 344, 494
———. 1994, Sol. Phys., 154, 1
November, L. J., & Simon, G. W. 1988, ApJ, 333, 427
November, L. J., Toomre, J., Gebbie, K. B., & Simon, G. W. 1981, ApJ, 245, L123
Petrovay, K., & Moreno Insertis, F. 1997, ApJ, 485, 398
Petrovay, K., & van Driel-Gesztelyi, L. 1997, Sol. Phys., 176, 249
Rimmele, T. R. 1997, ApJ, 490, 458
Rucklidge, A. M., Schmidt, H. U., & Weiss, N. O. 1995, MNRAS, 273, 491
Scharmer, G., Brown, D. S., Pettersson, L., & Rehn, J. 1985, Appl. Optics, 24, 2558
Schlichenmaier, R., Jahn, K., & Schmidt, H. U. 1998, ApJ, 493, L121
Shine, R. A., Title, A. M., Tarbell, T. D., Smith, K., & Frank, Z. 1994, ApJ, 430, 413
Shine, R. A., Title, A. M., Tarbell, T. D., & Topka, K. P. 1987, Science, 238, 1203
Simon, G. W., Brandt, P. N., November, L. J., Scharmer, G. B. & Shine, R. A. 1994, in Solar Surface Magnetism, ed. R. J. Rutten & C. J. Schrijver (Dordrecht: Kluwer), 261
Simon, G. W., & Leighton, R. B. 1964, ApJ, 140, 1120
Simon, G. W., & Weiss, N. O. 1970, Sol. Phys., 13, 85
Sobotka, M. 1985, Soviet Astron., 29, 576
———. 1997, in ASP Conf. Ser. 118, First Advances in Solar Physics Euroconference: Advances in the Physics of Sunspots, ed. B. Schmieder, J. C. del Toro Iniesta, & M. Vázquez (San Francisco: ASP), 155
Sobotka, M., Bonet, J. A., & Vázquez M. 1993, ApJ, 415, 832
———. 1994, ApJ, 426, 404
Sobotka, M., Bonet, J. A., Vázquez, M., & Hanslmeier, A. 1995a, ApJ, 447, L133
Sobotka, M., Brandt, P. N., & Simon, G. W. 1995b, in JOSO Annual Report 1995, ed. M. Saniga, 145
———. 1997a, A&A, 328, 682
———. 1997b, A&A, 328, 689
Soltau, D. 1994, in Solar Magnetic Fields, ed. M. Schüssler & W. Schmidt (Cambridge: Cambridge Univ. Press), 155
Strous, L. H. 1994, Ph.D. thesis, Univ. Utrecht
Strous, L. H., Scharmer, G., Tarbell, T. D., Title, A. M., & Zwaan, C. 1996, A&A, 306, 947

Sütterlin, P. 1998, A&A, 333, 305
Sütterlin, P., Schröter, E. H., & Muglach, K. 1996, Sol. Phys., 164, 311
Tarbell, T., Ferguson, S., Frank, S., Shine, R., Title, A., Topka, K., & Scharmer, G. 1990, in Solar Photosphere: Structure, Convection, and Magnetic Fields, ed. J. O. Stenflo (Dordrecht: Kluwer), 147
Title, A. M., & Berger, T. E. 1996, ApJ, 463, 797
Title, A. M., Tarbell, T. D., Topka, K. P., Ferguson, S., Shine, R. A., & SOUP Team. 1989, ApJ, 336, 475
Tönjes, K., & Wöhl, H. 1982, Sol. Phys., 75, 63
Topka, K. P., Tarbell, T. D., & Title, A. M. 1997, ApJ, 484, 479
van Driel-Gesztelyi, L., & Petrovay, K. 1990, Sol. Phys., 126, 285
Vrabec, D. 1974, in IAU Symp. 56, Chromospheric Fine Structure, ed. R. G. Athay (Dordrecht: Reidel), 201
Wang, H., & Zirin, H. 1992, Sol. Phys., 140, 41
Yi, Z., & Engvold, O. 1993, Sol. Phys., 144, 1
Zirin, H., & Wang, H. 1989, Sol. Phys., 119, 245
Zwaan, C. 1992, in Sunspots: Theory and Observations, ed. J. H. Thomas & N. O. Weiss (Dordrecht: Kluwer), 75
Zwaan, C., & Cram, L. E. 1989, in FGK Stars and T Tauri Stars, ed. L. E. Cram & L. V. Kuhi (NASA SP–502), 215